Article:
Billingsley, DJ, Lee, AJ, Johansson, NAB et al. (5 more authors) (2014) Patchiness of ion-exchanged mica revealed by DNA binding dynamics at short length scales. Nanotechnology, 25 (2). 02570. ISSN 1361-6528

https://doi.org/10.1088/0957-4484/25/2/025704

Patchiness of ion-exchanged mica revealed by DNA binding dynamics at short length scales

D J Billingsley[1,2], A J Lee[1], N A B Johansson[1], A Walton[1], L Stanger[1], N Crampton[1,2], W A Bonass[1,2], N H Thomson[1,2]

[1] *School of Physics & Astronomy, University of Leeds, Woodhouse Lane, Leeds, West Yorkshire, UK, LS2 9JT*

[2] *Department of Oral Biology, School of Dentistry, University of Leeds, Woodhouse Lane, Leeds, West Yorkshire, UK, LS2 9LU*

Email: n.h.thomson@leeds.ac.uk

Running Title: AFM study of DNA binding dynamics to mica

Abstract

The binding of double-stranded (ds) DNA to mica can be controlled through ion-exchanging the mica with divalent cations. Measurements of the end-to-end distance of linear DNA molecules discriminate whether the binding mechanism occurs through 2D surface equilibration or kinetic trapping. A range of linear dsDNA fragments have been used to investigate length dependences of binding. Mica, ion exchanged with Ni(II) usually gives rise to kinetically-trapped DNA molecules, however, short linear fragments (< 800bp) are seen to deviate from the expected behaviour. This indicates that ion-exchanged mica is heterogeneous, and contains patches or domains, separating different ionic species. These results correlate with imaging of dsDNA under aqueous buffer on Ni(II)-mica and indicate that binding domains are of the order of 100 nm in diameter. Shorter DNA fragments behave intermediate to the two extreme cases of 2D equilibration and kinetic trapping. Increasing the incubation time of Ni(II) on mica, from minutes to hours, brings the conformations of the shorter DNA fragments closer to the theoretical value for kinetic trapping, indicating that long time-scale kinetics play a role in ion-exchange. X-ray Photoelectron Spectroscopy (XPS) was used to confirm that the relative abundance of Ni(II) ions on the mica surface increases with time. These findings can be used to enhance spatial control of binding of DNA to inorganic surfaces with a view to patterning high densities arrays.

Introduction

Mica is a naturally abundant crystalline material present in the earth. Its anisotropic structure leads to interesting properties for different applications, including as an electrical and thermal insulator (Gray and Uher, 1977; Hackett and Morris, 1941; Hepburn *et al.*, 2000). It is an anhydrous clay-type mineral, where aluminium silicate layers 1nm thick are ionically bonded together; principally by K(I) ions in the case of Muscovite mica. There is a whole family of micas with different compositions, related in particular through substitutions of the aluminium atoms.

The weaker ionic bonding present between the dioctahedral layers, leads to almost perfect cleavage along the basal plane presenting a clean, atomically flat surface over mm^2. This property of mica, lends itself as an ideal substrate for microscopy. It is used as a support on which to evaporate thin carbon films for TEM and is used widely as a surface on which to deposit biomolecular and macromolecular samples for atomic force microscopy (AFM) (Thomson, 2006; Thomson *et al.*, 1996; Bustamante *et al.*, 1992; Hansma, 2001; Rivetti *et al.*, 2003).

When muscovite mica is cleaved, one expects half the interstitial K(I) ions to remain on each of the cleaved faces, retaining only 50% coverage of K(I) on the fresh surfaces (Muller and Chang, 1969). The distribution of the ions across these exposed surfaces is largely unknown but can be dynamic (Balmer *et al.*, 2007; Nishimura *et al.*, 1994; Loh and Jarvis, 2010; Sushko *et al.*, 2006). After cleavage, the exposed surfaces remain overall neutral but it is not at all clear whether the K(I) ions remaining on each face are evenly spaced, particularly after exposure to humid environments (Terashima, 2002).

Mica is a very hydrophilic surface (with a high surface energy) because the aluminium silicate layers are terminated in oxygen atoms and the K(I) ions are weakly bound (Gaines, 1957). Water completely wets the surface such that the contact angle is essentially zero and cannot be readily measured. This is a consequence of water molecules hydrogen bonding to the oxygen atoms, thought to create a strongly bound ice-like layer on which other water molecules can build up thicker and more mobile layers (Beaglehole and Christenson, 1992; Miranda *et al.*, 1998).

Exposure of mica to the ambient environment leads to dynamic changes to the surface chemistry as a consequence of water layers coming onto the surface. After weathering muscovite mica in air for a few hours or more, potassium carbonate crystallites form, where the mobile K(I) ions combine with carbon dioxide dissolving from the air into the surface water layers (Bhattacharyya, 1989; Christenson, 1985; Christenson, 1993; Christenson and Israelachvili, 1987). Ion-exchange of K(I) with H(I) ions in acidic solutions prevents formation of these crystals after subsequent air exposure (Christenson and Israelachvili, 1987).

For mica to be used as a support surface for biomolecular AFM it is often required that the K(I) ions are exchanged with another ionic species, usually a divalent metal cation, to encourage binding. In the simplest picture, this is thought to positively over-charge the surface and bind negatively-charged groups in the biomolecules, such as the phosphate backbone of double-stranded (ds) DNA.

The ability of divalent metal ions to replace K(I) ions is related to their enthalpy of hydration (Hansma and Laney, 1996), which is related in turn to their charge density and bonding orbitals. For example, exchanging with Mg(II) leads to dsDNA molecules that are surface equilibrated into 2D. By contrast, other ions, particularly transition metals, may lead to a kinetically-trapped molecule – essentially a 2D projection of the 3D conformation adopted in solution, where cross-overs of the DNA are allowed (Billingsley *et al.*, 2010; Pastre *et al.*, 2006; Pastre *et al.*, 2003). Pastre *et al.* modelled the DNA and mica surface as charged planes and hypothesized that if their respective counter-ions were to adopt a staggered configuration, they can be shared between the two surfaces (Pastre *et al.*, 2003). As such, correlations between the counter-ion clouds can lead to the situation where a net attraction exists between the DNA and mica, promoting the adsorption of the molecule (Pastre *et al.*, 2003; Pastre *et al.*, 2006). The DNA is physisorbed to the mica surface, and lateral diffusion of the molecules is inhibited by large frictional forces, related to electrostatic interactions between the two surfaces (Pastre *et al.*, 2005).

We hypothesize and demonstrate that exchanging the freshly cleaved surface of K(I)-mica with divalent metal ions, such as Ni(II), leads to a patchy charged surface where domains of K(I) and the exchanging ion are present in phase separated domains. This is based on the observed behaviours of dsDNA molecules in the AFM under Mg(II) containing buffer, absorbed to Ni-mica (i.e. muscovite mica pre-treated with a $NiCl_2$ solution). By careful study of the length dependence of dsDNA binding to mica and Ni-mica, we demonstrate that these patches exist and are ~120nm in diameter and that the unit cell periodicity for this 2D surface pattern is ~150nm. Better understanding of ion-exchange processes will enable greater control over patterning of the surface chemistry of mica at the nanoscale.

Materials and Methods

DNA fragment preparation

A range of differently sized linear DNA fragments were obtained and purified using different techniques. The 200, 400, 600 and 800 bp samples were obtained by amplifying different portions of a GAPDH cDNA template (1310 bp) with the polymerase chain reaction (PCR), using four specifically designed forward and reverses primers to obtain the necessary fragment sizes. The PCR reactions were performed using a GoTaq Hot Start Polymerase kit (Promega) by making up a 50 µl solution containing the heat resistant Taq polymerase (1.0 U), template DNA (3 fmol), dNTP mix (0.2 mM of each dNTP), and $MgCl_2$ (4 mM), and forward and reverse primers (0.4 µM). The reaction mix was then placed in a thermal cycler and 30 PCR cycles of denaturing (95 °C for 30s), annealing (55 °C for 60 s), and extension (72 °C for 60 s) were performed. The DNA fragments were purified using a QIAquick PCR purification Kit (Qiagen, Valencia, CA), as per the manufacturer's instructions.

The larger 1150 and 4300 bp fragments were isolated from plasmid pDSU (6136 bp). The plasmid underwent enzymatic digestion by HindIII (Promega) in Restriction enzyme buffer E (Promega) for two hours at 37 °C to produce four differently sized fragments. Gel electrophoresis stained with ethidium bromide was performed to separate the components by virtue of their different migration rates. The fragments of interest were visualized under UV light as a discreet band, and subsequently excised from the gel and purified using a QIAquick Gel Extraction Kit (Qiagen, Valencia, CA), as per the manufacturer's instructions.

Atomic force microscopy (AFM)

Following purification, all DNA samples were diluted tenfold in imaging buffer containing Tris-HCl (4 mM, pH 7.5) and 4 mM $MgCl_2$ to facilitate effective binding to the mica surface. Muscovite mica (Agar Scientific) was used as an imaging substrate for all DNA samples. This study called for each sample to be examined with and without pre-treatment of the mica with Ni(II) ions. Ion-exchange was carried out by transferring 30 µl of 2 mM $NiCl_2$ onto the surface. A standard incubation period of 10 minutes elapsed before the surface was rinsed with milliQ water to remove residual buffer salts, and dried with a weak flux of nitrogen gas. To investigate the kinetics of ion-exchange, the incubation time was also varied between 10 minutes and 24 hours.

DNA samples were prepared for AFM by depositing 10 µL of DNA solution onto freshly cleaved muscovite mica and incubating for 5 minutes at room temperature. After this, the samples were rinsed in milliQ water, before being dried in a weak flux of nitrogen gas. AFM images were collected in air with a Multimode Nanoscope III AFM (Veeco, Santa Barbara, CA) operating in Tapping Mode using silicon chips with an integrated cantilever (Olympus, Tokyo, Japan). Scans were collected at a scan line frequency of 2 Hz at 512 × 512 pixel resolution.

For imaging in liquid, a similar procedure for the sample preparation was followed, but after DNA incubation, the sample was not rinsed with water, it was introduced into the liquid cell of the AFM and imaged under the Tris-Mg buffer. Silicon nitride cantilevers of nominal spring constants in the range 0.1 to 0.4 N/m were indirectly acoustically excited at approximately 9 kHz. The samples were scanned in tapping mode at line rates of 2Hz.

Polymer Chain Statistics

Experimental measurements of DNA contour lengths were performed manually using the ImageJ software (NIH), by following the DNA backbone as a series of connected straight lines. For linear

DNA fragments, the end-to-end distances (R) were measured and a value of the mean square calculated using the Nanoscope software straight line measurement tool. The experimental values were compared to theoretical values for both surface equilibrated and kinetically trapped cases, calculated following the approach for polymer chain mechanics previously detailed in Rivetti *et al.*, 1996. For the surface equilibrated case, where the DNA chain is collapsed but free to move in the 2D plane of the surface, the mean square end-to-end distance $\langle R^2 \rangle_{2D}$ is predicted as;

$$\left\langle R^2 \right\rangle_{2D} = 4PL\left(1-\frac{2P}{L}(1-e^{\frac{-L}{2P}})\right) \qquad (1)$$

For kinetically trapped molecules the 2D surface conformation is a projection of the 3D conformation. The mean square end-to-end distance in 3D is given by;

$$\left\langle R^2 \right\rangle_{3D} = 2PL\left(1-\frac{P}{L}(1-e^{\frac{-L}{P}})\right) \qquad (2)$$

The projected mean square end-to-end by trigonometry becomes

$$\left\langle R^2 \right\rangle_{proj} = \left\langle R_x^2 \right\rangle + \left\langle R_y^2 \right\rangle = \frac{2}{3}\left\langle R^2 \right\rangle_{3D} \qquad (3)$$

The theoretical surface equilibrated values were calculated using Equation (1) and the kinetically trapped values using Equations (2) and (3). In both cases, it was assumed that the DNA persistence length (P) was equal to 53 nm (Bustamante *et al.*, 1994), and a base pair repeat of 0.33 nm was used to calculate the contour length (L). The persistence length, P, used in this analysis is that of the DNA in solution and not the apparent persistence length on a surface which can be affected by the DNA-surface interactions.

X-ray Photoelectron Spectroscopy (XPS)

Preparation of mica samples for XPS was carried out in exactly the same way as for the AFM studies. The samples were then transferred immediately into the XPS system for analysis. XPS was performed using a VG ESCALab 250 with a monochromated Al Kα source (500 μm spot size, 150W spot power). A low energy (2 eV) electron flood gun was used to compensate for surface charging during the experiments. Detailed scans of the K and Ni peaks were performed at a pass energy of 20 eV (constant analyser energy). The system was under UHV conditions (~10^{-10} mbar) during the experiments.

Results

Imaging linear DNA fragments (1074bp) bound to Ni-mica under bulk aqueous liquid by AFM, demonstrates that the standard preparation procedure of Ni(II) exchange at 2mM for 10 minutes, yields molecules which are not strongly bound along their whole contour length (Figure 1a). There are regions of the dsDNA that are strongly bound and do not move, and neighbouring regions that move back and forth across the surface and therefore are seen as regions of noise by conventional AFM with image acquisition times in the range of minutes (see Figure 1b). Over time, perturbations of one molecule can affect the position of a neighbouring molecule (Thomson, 2006).

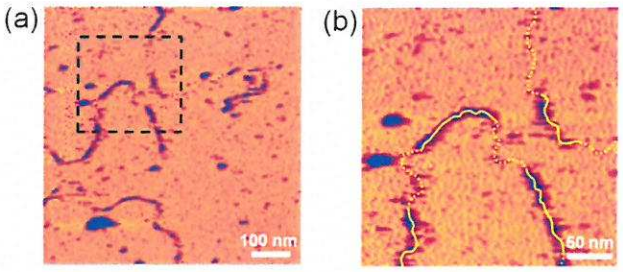

Figure 1. (a) DNA bound to Ni-mica imaged under bulk aqueous liquid by tapping-mode AFM. Certain regions of the chain appear strongly bound to the surface and are well resolved. However, neighbouring regions are weakly bound, appearing noisy. (b) Software zoom of the area bounded by the box in (a). To facilitate observation of the different binding strengths the DNA backbone has been traced out. Strongly bound segments are indicated by the solid line, and weakly bound regions by the dashed line.

The sizes of the two different regions were estimated by measuring the straight line end-to-end distance between two points on the DNA molecule from the start of a tightly-bound region to its end, and similarly with the segments that were weakly-bound. The typical sizes were found to be 126 ± 4 nm (n = 48) for the well-resolved segments and 121 ± 6 nm (n = 37) for the blurred regions. It is interesting to note that the sizes of the two regions are similar within errors.

The observation of alternating lengths of DNA, of approximate size 120 nm, led us to hypothesize that the surface is covered with Ni(II) domains of a given size and separation. The phase separation of ionic species bound to the mica surface can be schematically idealized as a polka dot pattern (Figure 2a). Under the conditions of our experiments, the space between the domains or Ni(II) dots will be occupied by ions of K(I), H(I) or Mg(II) in a dynamic equilibrium, the exact composition of which will depend on the solution conditions but is difficult to determine at the nanoscale. This composition, however, will be the same as that for mica which has not been pre-treated with Ni(II) (or other transition metal ions) under the same Tris-Mg DNA deposition buffer.

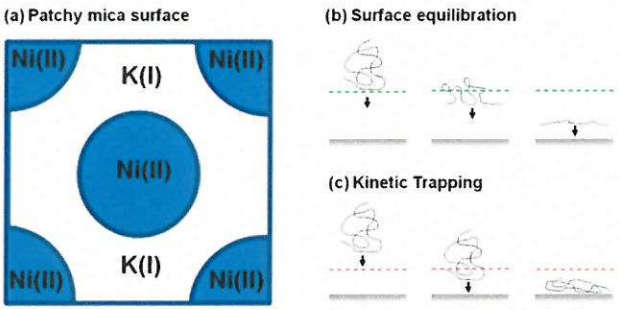

Figure 2. (a) Schematic diagram of an idealized polka dot structure of the ion-exchanged mica surface, shown containing a continuous region of K(I) and patches of Ni(II). The regions between the Ni(II) domains may be occupied by various ionic species present in the deposition buffer, also including H(I) and Mg(II). (b) Schematic diagram of the adsorption mechanisms of DNA onto mica substrate from solution. Surface equilibration is governed by long-ranged interactions (shown by green dashed line). The molecule takes up a flat minimum energy conformation. (c) Short-range forces (indicated in red) are responsible for kinetic trapping. The interaction is much stronger, with the molecule being pinned at one or more locations and its remaining segments collapsing around it.

We decided therefore to probe the heterogeneity of Ni-mica through the binding behaviour and conformations of different length fragments of double-stranded DNA. Measurements of the straight line end-to-end distance (R) for a range of lengths of linear DNA molecules (200 bp to 4.3 kbp) on air dried samples were performed. See Figure 3 for example AFM images of each fragment size for the two preparation methods. We compared the measured average end-to-end squared $\langle R^2 \rangle$ values for the DNA on freshly cleaved mica, and Ni-mica with calculated theoretical values (Table I and Figure 4). As expected, on mica in the Mg(II) containing deposition buffer, the experimental measurements

closely followed the theoretical trend for 2D surface equilibration, as previously observed by Rivetti et al. (Rivetti *et al.*, 1996) (See Figure 2b and Figure 4a). On Ni-mica, the longer DNA molecules (>800 bp) closely follow the trend for kinetically-trapped molecules, as previously observed (Billingsley *et al.*, 2010) (See Figure 2c and Figure 4b).

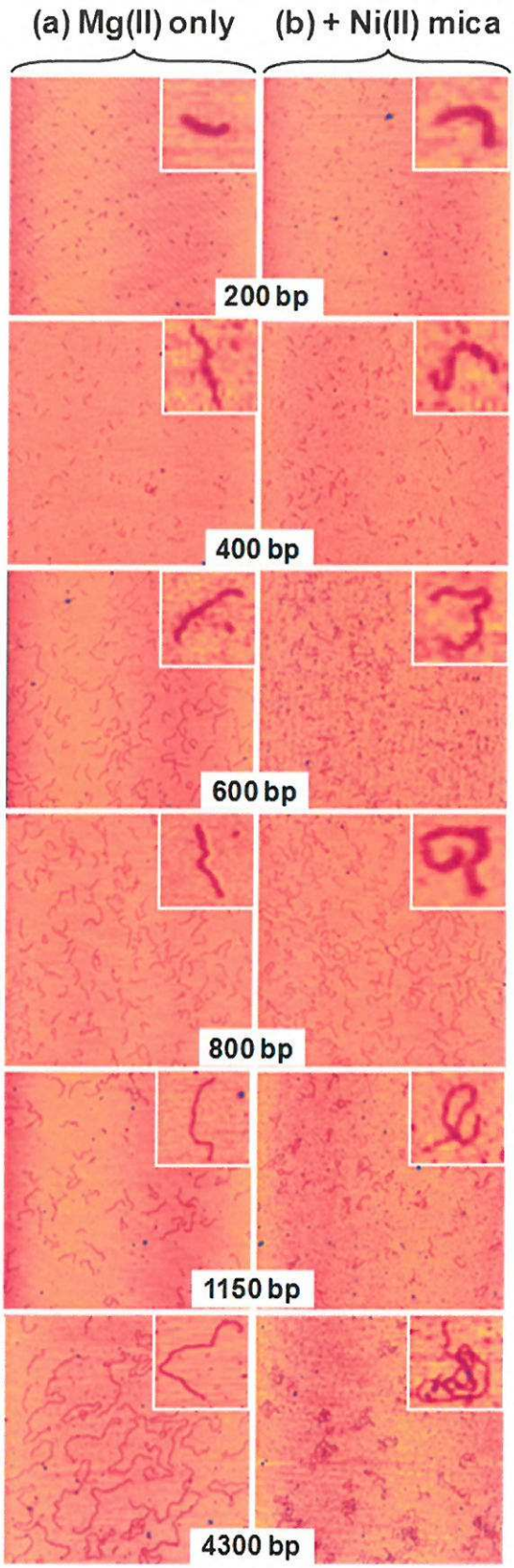

Figure 3. Typical AFM images of each fragment prepared with (a) Mg(II) only (left column), and (b) additional Ni(II) pre-treatment of mica (right column). Each image is 3 μm × 3 μm. An example of each length at each preparation method is shown in the inset of each image.

Table 1. Experimentally measured values of average square end-to-end distance $\langle R^2 \rangle$ for DNA fragments of different sizes prepared with Mg(II) in buffer, either on mica or mica with Ni(II) pre-treatment (n ranges from 74 to 240). These experimental values are compared with the theoretical values for surface equilibration $\langle R^2 \rangle_{2D}$ and kinetic trapping $\langle R^2 \rangle_{proj}$.

DNA Fragment Size (bp)	Surface Equilibration $\langle R^2 \rangle_{2D}$ Equilibrated theoretical (nm^2)	Surface Equilibration $\langle R^2 \rangle$ Experimental: Mg(II) only (nm^2)	Surface Equilibration σ (nm^2)	Kinetic Trapping $\langle R^2 \rangle_{proj}$ Trapped theoretical (nm^2)	Kinetic Trapping $\langle R^2 \rangle$ Experimental: + Ni (II) (nm^2)	Kinetic Trapping σ (nm^2)
200	3,577	3,047	766	1,997	3,638	785
400	11,981	11,210	3,103	5,893	7,865	4,072
600	22,975	22,956	8,248	10,336	11,225	8,363
800	35,358	35,901	15,045	14,936	15,022	10,497
1150	58,608	54,867	28,230	23,076	22,890	19,193
4300	278,356	306,955	249,629	96,531	99,431	84,610

However, for the Ni-mica case, once the contour length goes below < 800bp significant deviation from the kinetically trapped form is observed (Figure 4b and Table 1). The observed end-to-end distances begins to approach a value that is intermediate between being kinetically trapped and 2D surface equilibrated. At the smallest fragment size (200 bp) tested, the end-to-end distance for Ni(II) prepared samples deviates from ideal kinetic trapping further still, and actually agrees closely with a value typical of 2D surface equilibration (see top row, Table I).

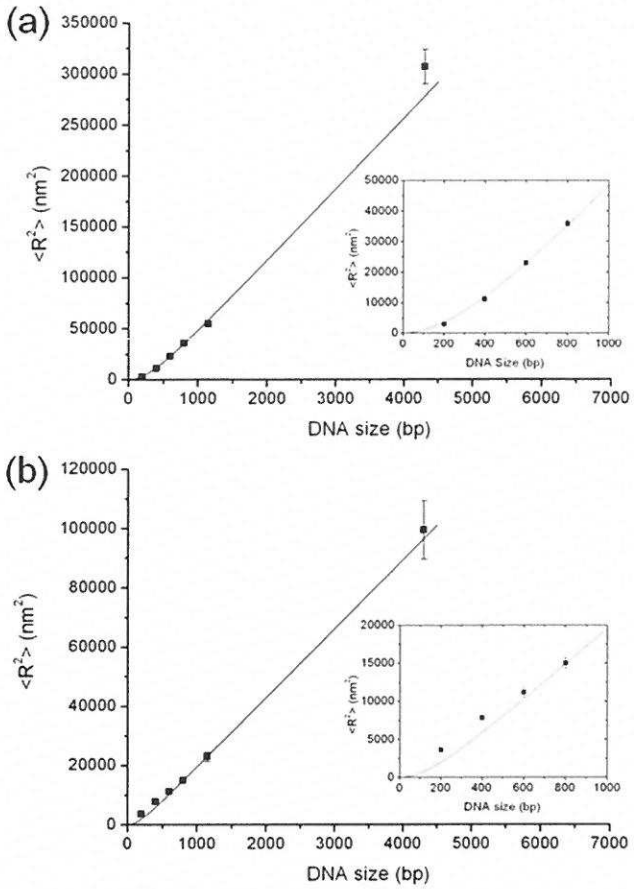

Figure 4. (a) Experimental values of mean square end-to-end distances (filled squares) of samples prepared with Mg(II) alone, plotted with a curve of the theoretical values for surface equilibration $\langle R^2 \rangle_{2D}$. The inset shows a close-up of the region from 0-1000 bp where most of the measurements are clustered. (b) Experimental values of mean square end-to-end distances (filled squares), of samples prepared with Ni(II) pre-treatment of mica, plotted with a curve of the theoretical values for kinetic trapping $\langle R^2 \rangle_{proj}$. The inset shows a close-up of the region from 0-1000 bp. Below a fragment size of 800 bp the points begin to deviate from the theoretical prediction. The magnitude of the difference increases toward smaller fragment size. Errors bars are the standard error in the mean of the distributed values of $\langle R^2 \rangle$.

As the length of the DNA decreases, the deviation away from kinetic trapping towards conformations indicating 2D equilibration becomes more marked. Taken together with the dynamic imaging under liquid, these data indicate that the hypothesis of an ion-exchanged mica surface with localized patches of Ni(II) ions is a realistic one. We wanted to test therefore, whether we could alter the size of the ion-exchanged patches on mica by varying the incubation time.

Ion-exchange on the surface of mica for different ion species will be time dependent. To investigate whether increasing the incubation time of the Ni(II) above mica leads to greater ion exchange with the surface, we used X-ray Photoelectron Spectroscopy (XPS) to confirm if the amount of nickel on the surface was increasing. Samples exchanged at the usual time course of 10 minutes were compared those against mica exchanged with Ni(II) solution for 24 hours. Since the Ni(II) is present at sub-monolayer concentrations, a long time incubation of 24 hours was chosen to ensure a measurable change in the XPS. The penetration depth of the X-rays is of the order of several nanometres, so it is difficult to measure the mica surface Ni/K ratio directly, since K is in the mica lattice and Ni is not. The results show, however, that the absolute amounts of Ni(II) on the mica surface have increased (Table 2). Taking into account the relative sensitivity factors for each of the peaks, the percentage of Ni relative to K for 10 min and 24 hour incubations are 3.8 and 4.5%, respectively (± 0.1). Overall, the XPS data revealed that by increasing the incubation time the amount of Ni on the mica increases.

Table 2. XPS data for different Ni(II) incubation times.

	Area under peak (Cps.eV) and standard deviations			
Sample	**K 2p**	$\sigma_{(K)}$	**Ni 2p3**	$\sigma_{(Ni)}$
Bare mica	19.22	0.07	-0.08	0.08
Mica + 10 mins Ni(II) incubation	13.92	0.06	1.92	0.06
Mica + 24 hours Ni(II) incubation	13.86	0.06	2.30	0.06

To investigate further, we carried out an AFM study of varying the pre-treatment incubation time of Ni(II) above the mica surface between 10 minutes and 24 hours. Qualitatively we found that as the incubation time increased there was a greater amount of nano-particulates in the background of the AFM images. These are likely to be nanocrystallites of nickel hydroxide which precipitate around pH 8 (Hsueh *et al.*, 2001). This effect became very pronounced after 3 hours incubation time, to the extent that these features obscured imaging of the DNA molecules on the surface (data not shown).

To study whether the Ni(II) domain size increased before the crystallisation processes took over, we restricted a detailed AFM study into the kinetics of Ni(II) exchange with the mica up to 6 hours. For the 400bp DNA, which is in the middle of the length range where the deviation from the expected scenario occurs, one observes a progressive decrease in the $\langle R^2 \rangle$ value over a period of ~2 hours before it stabilizes close to the theoretical value for the kinetically trapped conformation (Figure 5).

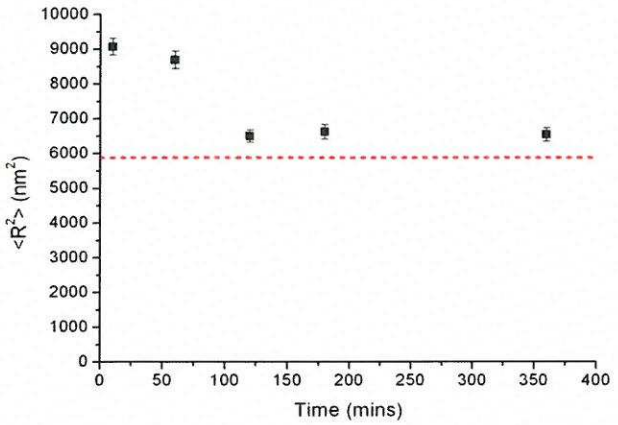

Figure 5. Experimental values of average square end-to-end distance $\langle R^2 \rangle$ for 400 bp DNA deposited on Ni(II) ion-exchanged mica prepared at increasing Ni(II) incubation times. The theoretical $\langle R^2 \rangle$ value for a kinetically-trapped fragment of 400bp is shown by a dashed line. At short ion-exchange times the experimental points do not agree with the theoretical case. However, as the incubation period is increased beyond two hours the measured points stabilize and approach values much closer to the theoretical one. Errors bars are the standard error in the mean of the distributed values of $\langle R^2 \rangle$.

We therefore, carried out the length dependence study again for DNA fragments 800bp or below, for 2 hours Ni(II) incubation and compared it with the standard 10 minute incubation time (Figure 6). For all the shorter size fragments (200, 400, 600 bps) the $\langle R^2 \rangle$ values on Ni-mica that were produced by a 2 hour incubation, were consistently lower than those at the short time-scale, indicating that the domain size of the Ni(II) islands or patches had increased. Interestingly, as the DNA fragment size decreases from 600 to 200bp, it becomes more difficult to obtain all the molecules on the surface in the kinetic trapped configuration.

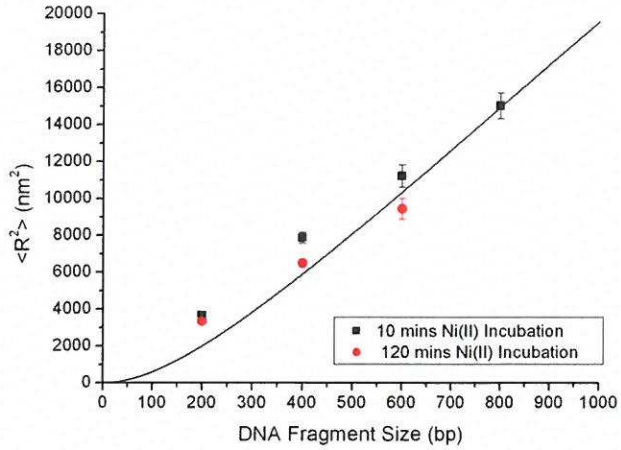

Figure 6. Effect of increased Ni(II) incubation time for DNA fragments of size 200-600 bp. Previous experimental values of $\langle R^2 \rangle$ are shown by black squares, whilst the effect of increased two hour incubation is shown by red circles. The theoretical values for an ideal kinetically trapped fragment are displayed by the curve. In all cases, the longer time period leads to smaller end-to-end distances, with most fragments approaching the theoretical case. Errors bars are the standard error in the mean of the distributed values of $\langle R^2 \rangle$.

It is conceivable that the presence of Ni(II) domains could lead to regions of high local charge density, which might affect the local properties of the DNA molecules. For example, a change in overall molecular contour length would lead to a corresponding variation in the end-to-end distance that might lead to an apparent deviation in idealized kinetic trapping behaviour. To investigate this possibility, contour length measurements were made for fragments of sizes 200 bp to 1150 bp for each preparation method (Table 3). We observed no statistically significant differences in contour length for any fragments for either of the two surface binding strategies. Additionally, the corresponding values of the helical rise per bp, indicate that the molecules exist on the surface as B-form DNA. This shows that the variations in $\langle R^2 \rangle$ do not result in local variations of DNA properties such as a change in the helical pitch and resultant contour length, but rather a change in global conformation and surface binding behaviour.

Table 3. Measured values of contour length for DNA fragments of different sizes prepared with Mg(II) in buffer, either on mica or mica with Ni(II) pre-treatment (n ranges from 100 – 105). The helical rise per bp was calculated from each contour length measurement divided by the length in bps.

	Mg(II) only			+ Ni(II) mica		
DNA Fragment (bp)	Contour Length (nm)	σ (nm)	Base pair repeat (nm)	Contour Length (nm)	σ (nm)	Base pair repeat (nm)
200	67.25	4.60	0.34 ± 0.02	69.10	5.42	0.34 ± 0.03
400	128.69	6.62	0.32 ± 0.02	130.97	6.70	0.32 ± 0.02
600	193.84	15.49	0.32 ± 0.03	192.76	19.07	0.32 ± 0.03
800	251.68	11.79	0.32 ± 0.01	253.45	12.52	0.33 ± 0.02
1150	385.17	27.24	0.33 ± 0.02	384.09	17.39	0.33 ± 0.02

Discussion

All the AFM data taken together can be explained if the ionic exchange process is separated into localized patches or islands. The liquid AFM imaging shows that the DNA is not firmly bound to the mica along the whole contour length for DNA fragments of ~1000bp. This is characteristic of binding mediated by Mg(II) ions, where these counter-ions are in dynamic equilibrium with the Mg(II) ions in solution.

The layers in mica are bound together via weak ionic interactions mediated by K(I) ions, which are able to fit into small recesses above the OH groups buried in the mica surface. It has been suggested that when the mica surface becomes hydrated some K(I) ions can be released into solution, leaving the surface negatively charged (Pashley, 1981). The vacancies left behind by K(I) can be filled by ions of similar size, that are present in the solution (Hansma and Laney, 1996; Nishimura *et al.*, 1994). In the case of the surface pre-treatment attempted here, this will be Ni(II) present in the $NiCl_2$ solution. The cleaving of the top mica layer is expected to remove half of the K(I) ions on the uppermost cleaved layer, leaving the freshly clean surface half occupied (Muller and Chang, 1969). If these ions are not immediately exchanged once $NiCl_2$ is added to the surface, then the Ni(II) ions would only be able to fill half the surface sites: those that are unoccupied. Since the solution above the mica contains both H(I) and Mg(II) ions, these ions are also competing to displace the K(I) ions. The behaviour of DNA indirectly reveals that the binding sites on the mica surface are not homogeneously distributed.

The fact that every $\langle R^2 \rangle$ point for samples prepared with only the Mg(II) buffer agrees with the theoretical binding curve shows that there is a homogeneous distribution of magnesium ions on the surface and the DNA. As such, all molecules behave similarly and the ensemble average of $\langle R^2 \rangle$ tends to the theoretical value, representing surface equilibrated molecules. There is no length dependence, and small fragments are able to equilibrate in an identical way to longer chains.

It is important to note that pre-treating mica with Mg(II) only, without including it in the deposition buffer does not allow DNA to bind reliably to the mica surface. During a rinsing step with water, the DNA and Mg(II) ions are flushed from the surface. This indicates that Mg(II) ions are in dynamic equilibrium with the mica binding sites on time-scales shorter than seconds. This is symptomatic of group II divalent cations which cannot form directional bonding with the sub-surface OH groups in mica, because they have no half-filled d-orbitals.

For transition metal cations, such as Ni(II), ligands can form directional strong bonds to the d-orbitals with long life-times. For Ni(II)-mica, the $\langle R^2 \rangle$ values show an increasing deviation from an ideal kinetically trapped case, below a certain DNA size threshold. This change in binding occurs somewhere between 800 bp and 600 bp, after which the DNA exists in an intermediate conformation that is between kinetically trapped and surface equilibrated. As this effect is dependent on chain length, it indicates that the surface properties of the Ni(II)-mica are heterogeneous on a similar length scale.

Observation of deviation from kinetic trapping below a certain transition point in DNA length indicates that the patches of ions are smaller in effective diameter than the DNA contour length. The change in ideal behaviour is seen below chain lengths of roughly 267 nm (800 bp). Additionally, the fact that the deviation from the expected values of $\langle R^2 \rangle$ increases as the fragment size decreases, suggests that the size of the Ni(II) patches begins to approach that of the DNA chain length. We have idealized the surface structure to that of patch charge distribution of Ni(II) polka dots in a "sea" of mica that is undergoing dynamic ion-exchange between K(I), H(I) and Mg(II) ions (Figure 7). For the longer DNA fragments (> 800bp), the molecules span these patches and because the patch size is much smaller than the fragment length their overall mode of binding is kinetic trapping, where the instantaneous pinning of the DNA backbone during interaction with the bound Ni(II) dominates. For fragments of similar size to the patches (~ 800bp) the probability that the molecules can bridge the patches decreases. For even shorter fragments, it becomes possible for molecules to be either fully bound to the Ni(II) patch (i.e. kinetically trapped) or fully bound to the inter-patch region (i.e. surface equilibrated) (see Figure 7b). This could explain why the fractional deviation from the expected case increases for smaller DNA fragments.

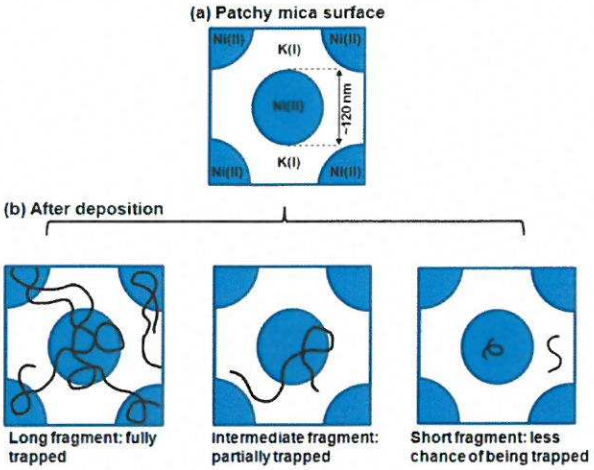

Figure 7. Schematic diagram of an idealised possible structure of the ion-exchanged mica surface, containing regions of K(I) and patches of Ni(II). (a) The unit cell of a periodic polka dot pattern would be ~250nm across based on the experimental observations. (b) Representations of how different length DNA fragments appear on the surface. Longer fragments can bind easily across more than one region of Ni(II), meaning they are fully trapped. As the fragments become shorter there is less of the chance of a molecule interacting with a Ni(II) region. As such, there are less fully trapped molecules and a corresponding increase in mean square end-to-end distance.

As yet, it is unknown why during cleavage the mica should retain regions where the K(I) ions on each surface remain clustered together. It might arise from the surface electric field distributions during the cleavage process. Charge patches are common in electrostatic systems and arise from the trade-off in energies between the electrostatic energy of the patch with the line tension of the edge of the patch. Heterogeneous surface charge properties have been observed on a related mica mineral known as brucite, which can affect the conformation of the DNA, stretching out the entropic coil and bridging long DNA molecules between regions of positive charge (Antognozzi *et al.*, 2006). This effect was explained by the long range electric field distributions in the solution above the surface influencing the conformation and binding of the DNA.

The fact that we see the onset of the deviation from ideal kinetically trapped behaviour below 800 bp allows us to make an estimate of the size of the Ni(II) domains (Figure 7a). DNA has shown to be a semi-flexible polymer and can be modelled as a worm-like chain. The radius of gyration R_G can be estimated for a worm-like-chain polymer, such as DNA, by using the formula, $\langle R_G \rangle = \sqrt{2 l_c l_p}/\sqrt{6}$, where l_c is the contour length of chain and l_p is the persistence length. By using a value for the persistence length of 53 nm and a base pair repeat of 0.332 nm to calculate the contour length, we can obtain an estimate of $\langle R_G \rangle$ for a 800 bp DNA chain of 67.6 nm; making the effective diameter of the object 135.2 nm. This value compares favourably with the size of the different binding domains observed during imaging in bulk aqueous fluid. As such, these values provide an estimate of the size of the Ni(II) domains.

Increasing the Ni(II) incubation time led to a reduction in $\langle R^2 \rangle$, which represents the time dependant kinetics of the ion exchange upon the mica surface, and illustrates that the surface properties are tunable. Results on the 400 bp fragment indicate that the fragments were fully kinetically trapped after a two hour period of surface pre-treatment (Figure 5). Longer incubation times (2 hours) led to other fragments agreeing much better with a kinetically trapped model for binding (Figure 6). This correlates with an increased amount of Ni(II) ions on the surface, as demonstrated by XPS data. Terashima *et al.* measured the weight of mica before and after immersion in water by use of an ultramicrobalance, and found a decrease in weight due to ion exchange of K(I) ions, which took 30 minutes to achieve full dissolution under those conditions (Terashima, 2002). Longer incubation times led to appearance of large particulates on the surface, and is attributed to the crystallization of Ni(II)

compounds. It is known that metal ions in solution possess complex speciation properties. Hsueh *et al.* studied the physicochemical properties of nickel treated mica at the nanoscale (Hsueh *et al.*, 2001). Using AFM they were able to show that molecular monolayers can form on mica treated with aqueous $NiCl_2$, and was likely a result of metal or metal hydroxide precipitates. Thermodynamic simulations demonstrated that nickel ion speciation is highly sensitive to pH in the range 6-8, and that Ni(II) ions are able to form stable solid precipitates of $Ni(OH)_2$.

In the same study they were also able to show that DNA bound to nickel treated mica could be cleaved *in situ* using the restriction enzyme RsaI (Hsueh *et al.*, 2001). Typically, 30-40% of recognition sites were cleaved, indicating that the adsorbed DNA retains some mobility to permit the enzyme access to the bases via the major groove. It was suggested that there is a balance between tight binding to the surface and local areas of flexibility, as would arise if not all Ni(II) binding sites on the mica surface were occupied. This provides further evidence that the mica surface is organised into domains of different ionic species.

The binding of DNA onto inorganic surfaces, such as mica, is controlled by the electrostatics of the interaction, its spatial distribution and interplay with the fluctuating dynamics of the DNA molecule. Our study indicates that these interactions can be modulated to a certain extent, possibly enough to produce patterning of DNA on the nanoscale on insulating surfaces. A recent approach to actively control DNA adsorption onto conducting HOPG surfaces through an applied surface potential was recently demonstrated (Doi *et al.*, 2013). This further opens up the possibilities to produce patterns of biomolecules, including DNA, with nanoscale structural features on technologically important surfaces.

Finally, the idea of an ionic patchwork on the surface mica after cleavage has been proposed previously (Campbell *et al.*, 1998). This was postulated on the observation of dynamic 0.1 nm high steps on the mica as detected by AFM. These steps are too small to be the c-direction height of the crystallographic unit cell and were proposed as domains of K(I) ions. Our work supports this conclusion giving further strong evidence of mica surface heterogeneity after cleavage and revealing the long time-scales that can be involved in ion exchange.

Conclusions

Through the binding behaviour, dynamic imaging and final conformations of DNA molecules on mica surfaces, it is demonstrated that muscovite mica ion-exchanged with transition metal ions, such as Ni(II), is heterogeneous and phase-separated into patches. The size of the patches is on the nanoscale (~ 100nm) and influences the binding of the DNA at short length scales (<800bp). We expect this to be a general behaviour of transition metal ions that can bind strongly to the OH groups within the mica surface through directional ligand bonds of their d-orbitals. This strong directional bonding localizes the ions on the surface, in contrast to group II divalent cations, such as Mg(II). The appearance of two characteristic time-scales of ion-exchange, i.e. the inability of Ni(II) to replace the K(I) ions on the minute time-scale, suggests that K(I) ions are not as readily exchanged as previously expected and that the Ni(II) ions typically occupy the 50% of empty sites on the mica surface after initial cleavage. The work reveals that the ion-exchange processes on mica are not necessarily homogeneous. This has important implications for the use of mica as a crystallisation substrate or a surface for macromolecular nano-patterning using soft lithography techniques, such as micro-contact printing.

Acknowledgements

We thank Fiona Hurrell for acquisition of the DNA images under bulk aqueous liquid. We also thank Hugo K Christenson for important discussions on the kinetics of ion-exchange on mica, crystallisation processes on mica and the water layer thicknesses. We acknowledge funding from the EPRSC for DJB (EP/G500010/1), AJL (EP/J500124/1) and AW (EP/F056311/1) and the University of Leeds.

References

Antognozzi M, Wotherspoon A, Hayes J M, Miles M J, Szczelkun M D and Valdre G 2006 A chlorite mineral surface actively drives the deposition of DNA molecules in stretched conformations *Nanotechnology* **17** 3897-902

Balmer T E, Christenson H K, Spencer N D and Heuberger M 2007 The effect of surface ions on water adsorption to mica *Langmuir* **24** 1566-9

Beaglehole D and Christenson H K 1992 Vapor adsorption on mica and silicon - entropy effects, layering, and surface forces *J. Phys. Chem.* **96** 3395-403

Bhattacharyya K G 1989 Adsorption of carbon dioxide on mica surfaces *Langmuir* **5** 1155-62

Billingsley D J, Kirkham J, Bonass W A and Thomson N H 2010 Atomic force microscopy of DNA at high humidity: irreversible conformational switching of supercoiled molecules *Physical Chemistry Chemical Physics* **12** 14727-34

Bustamante C, Marko J F, Siggia E D and Smith S 1994 Entropic elasticity of lambda-phage DNA *Science* **265** 1599-600

Bustamante C, Vesenka J, Tang C L, Rees W, Guthold M and Keller R 1992 Circular DNA-molecules imaged in air by scanning force microscopy *Biochemistry (Mosc).* **31** 22-6

Campbell P A, Sinnamon L J, Thompson C E and Walmsley D G 1998 Atomic force microscopy evidence for K+ domains on freshly cleaved mica *Surface Science* **410** 768-72

Christenson H K 1985 Capillary condensation in systems of immiscible liquids *J. Colloid Interface Sci.* **104** 234-49

Christenson H K 1993 Adhesion and surface energy of mica in air and water *The Journal of Physical Chemistry* **97** 12034-41

Christenson H K and Israelachvili J N 1987 Growth of ionic crystallites on exposed surfaces *J. Colloid Interface Sci.* **117** 576-7

Doi K, Takeuchi H, Nii R, Akamatsu S, Kakizaki T and Kawano S 2013 Self-assembly of 50 bp poly(dA)·poly(dT) DNA on highly oriented pyrolytic graphite via atomic force microscopy observation and molecular dynamics simulation *The Journal of Chemical Physics* **139** 085102

Gaines G L 1957 The Ion-exchange Properties of Muscovite Mica *The Journal of Physical Chemistry* **61** 1408-13

Gray A S and Uher C 1977 Thermal-conductivity of mica at low-temperatures *Journal of Materials Science* **12** 959-65

Hackett W and Morris T A 1941 The electric strength of mica and its variation with temperature *Journal of the Institution of Electrical Engineers* **88** 295-303

Hansma H G 2001 Surface biology of DNA by atomic force microscopy *Annu. Rev. Phys. Chem.* **52** 71-92

Hansma H G and Laney D E 1996 DNA binding to mica correlates with cationic radius: Assay by atomic force microscopy *Biophys. J.* **70** 1933-9

Hepburn D M, Kemp I J and Shields A J 2000 Mica *Ieee Electrical Insulation Magazine* **16** 19-24

Hsueh C, Chen H, Gimzewski J K, Reed J and Abdel-Fattah T M 2001 Localized Nanoscopic Surface Measurements of Nickel-Modified Mica for Single-Molecule DNA Sequence Sampling *ACS Applied Materials & Interfaces* **2** 3249-56

Loh S-H and Jarvis S P 2010 Visualization of Ion Distribution at the Mica Electrolyte Interface *Langmuir* **26** 9176-8

Miranda P B, Xu L, Shen Y R and Salmeron M 1998 Icelike water monolayer adsorbed on mica at room temperature *Physical Review Letters* **81** 5876-9

Muller K and Chang C C 1969 Electric dipoles on clean mica surfaces *Surface Science* **14** 39-51

Nishimura S, Biggs S, Scales P J, Healy T W, Tsunematsu K and Tateyama T 1994 Molecular-scale structure of the cation modified muscovite mica basal-plane *Langmuir* **10** 4554-9

Pashley R M 1981 DLVO and hydration forces between mica surfaces in Li+, Na+, K+, and Cs+ electrolyte solutions: A correlation of double-layer and hydration forces with surface cation exchange properties *J. Colloid Interface Sci.* **83** 531-46

Pastre D, Hamon L, Landousy F, Sorel I, David M O, Zozime A, Le Cam E and Pietrement O 2006 Anionic polyelectrolyte adsorption on mica mediated by multivalent cations: A solution to DNA imaging by atomic force microscopy under high ionic strengths *Langmuir* **22** 6651-60

Pastre D, Pietrement O, Fusil P, Landousy F, Jeusset J, David M O, Hamon C, Le Cam E and Zozime A 2003 Adsorption of DNA to mica mediated by divalent counterions: A theoretical and experimental study *Biophys. J.* **85** 2507-18

Pastre D, Pietrement O, Zozime A and Le Cam E 2005 Study of the DNA/ethidium bromide interactions on mica surface by atomic force microscope: Influence of the surface friction *Biopolymers* **77** 53-62

Rivetti C, Guthold M and Bustamante C 1996 Scanning Force Microscopy of DNA Deposited onto Mica: Equilibration versus Kinetic Trapping Studied by Statistical Polymer Chain Analysis *J. Mol. Biol.* **264** 919-32

Rivetti C, Guthold M, Sankar L A and Susan G 2003 Single DNA Molecule Analysis of Transcription Complexes *Methods Enzymol.* **371** 34-50

Sushko M L, Shluger A L and Rivetti C 2006 Simple model for DNA adsorption onto a mica surface in 1 : 1 and 2 : 1 electrolyte solutions *Langmuir* **22** 7678-88

Terashima H 2002 A direct measurement of the ion-exchange capacity of muscovite mica using a Mettler ultramicrobalance *J. Colloid Interface Sci.* **245** 81-5

Thomson N H 2006 *Applied Scanning Probe Methods Vol VI: Characterization,* ed B Bhushan, *et al.* (Berlin: Springer-Verlag)

Thomson N H, Kasas S, Smith B, Hansma H G and Hansma P K 1996 Reversible binding of DNA to mica for AFM imaging *Langmuir* **12** 5905-8